Propagation and Coupling Characteristics of Microstrip Lines with Laminated Ground Plane

Jean-Fu Kiang, *Member, IEEE*

Abstract— **In this paper, we analyze the effect of laminated ground plane on the propagation and coupling characteristics of microstrip lines. Each lamina is modeled as an anisotropic layer, and transition matrix is used to relate the tangential field components in different laminae. An integral equation is formulated in the spectral domain, and the Galerkin's method is applied to solve the integral equation for the phase and the attenuation constants of several microstrip line structures. The effects of substrate dielectric are also studied. The attenuation constant variation thus obtained will be useful in circuit board design and in studying signal transmission in lamina environment.**

I. Introduction

IN SOME MODERN multilayer circuit board designs, perforations are fabricated in the ground plane to improve the adhesion between the substrates and the ground plane with temperature variation. The designer can also route vias through these perforations without punching holes in the ground plane. Propagation characteristics with periodically perforated ground plane have been analyzed by several authors [1]–[3]. In [1] and [2], integral equations were derived based on the electric surface current on the metal surface. In [3], the authors used electric surface current on the microstrip line and used magnetic surface current on the perforations as field sources. These approaches worked well when the perforation size is comparable to wavelength in the medium. If the microstrip is much wider than the perforation dimension, too many unknowns are needed to model surface currents.

Some ground planes are fabricated by laying one layer of metallic wires over the substrate followed by another layer of wires perpendicular to the first layer. Hence, such ground plane can be treated as two stacking layers of anisotropic media. In each wire layer, the conductivity along the wire orientation is much higher than the perpendicular orientations.

Scattering from sandwiched layer of conducting fibers has been analyzed in [4]. The fiber spacing is comparable to wavelength, hence Floquet modes are incorporated in the analysis. In [5], an anisotropic conductivity tensor is used to study the shielding effectiveness of a G/E lamina which is an epoxy resin embedding graphite fibers. G/E lamina and similar composites have been widely used in aerospace industry. The fiber separation in the G/E lamina is a tiny fraction of a wavelength, hence using an equivalent conductivity tensor is appropriate to analyze its propagation properties.

Recently, anisotropy and inhomogeneity of the circuit board have been considered in the analysis of high speed digital transmission [6], [7]. In [7], a differential matrix operator is derived from Maxwell's equations to calculate the tangential field components. This method was also used in optics [8], [9], and scattering [10]. General derivation can also be found in [11] and [12].

With either perforated ground plane or laminated ground plane, the propagation characteristics are different from that obtained by the solid ground plane assumption. We assume that the wire/fiber spacing in each lamina of the ground plane is much smaller than a wavelength, hence each lamina can be modeled as an anisotropic layer with a conductivity tensor. Leakage through the laminated ground plane will cause coupling between two microstrip lines on opposite sides of the ground plane. The coupling induces difference of phase and attenuation constants between the even and the odd modes.

Microstrip phased array with microstrip line feeding structure has been built on aircraft surface [13]. Similar array may be mounted on modern aircrafts where composite material is used. Hence, it is very important and practical to understand the propagation characteristics of microstrip line on laminated composite ground plane.

We will first formulate a transition matrix, and then derive an integral equation based on the electric surface current on the microstrip lines. Galerkin's method is applied to solve for the phase and attenuation constants of given microstrip line structures. Next, we apply the same procedures to study the propagation properties of two coupled microstrip lines.

II. Transition Matrix

As shown in Fig. 1, a microstrip line is printed on the surface of substrate layer (1). The ground plane is made of laminae with each lamina described by an effective permittivity tensor and an effective conductivity tensor. If more shielding effectiveness is required, we may bind more laminae or choose material of higher conductivity to form the ground plane.

We first derive a transition matrix for waves in anisotropic layers. Assume that all layers are stacked along the z direction, the effective permittivity $(\bar{\bar{\epsilon}})$ and conductivity $(\bar{\bar{\sigma}})$ tensors in each layer are independent of z. If the principal axis of $\bar{\bar{\sigma}}$ and

Manuscript received November 10, 1994, revised November 12, 1995. This work was supported in part by the National Science Council, ROC, Project NSC85-2213-W005-010.

The author is with Department of Electrical Engineering, National Chung-Hsing University, Taichung, Taiwan, ROC.

Publisher Item Identifier S 0018-9480(96)01445-7.

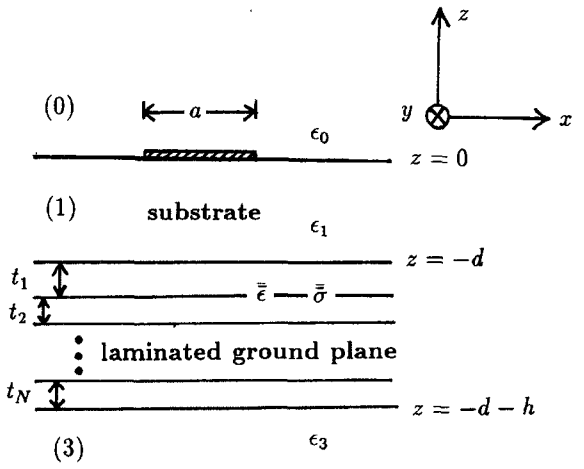

Fig. 1. A microstrip line in the presence of laminated ground plane.

$\bar{\bar{\epsilon}}$ skews from the x axis by an angle α (when the wires or fibers are embedded with an angle α with the x axis), $\bar{\bar{\sigma}}$ and $\bar{\bar{\epsilon}}$ can be expressed as

$$\bar{\bar{\sigma}} = \begin{bmatrix} \bar{\bar{\sigma}}_s & 0 \\ 0 & \sigma_{zz} \end{bmatrix} = \begin{bmatrix} \sigma_{xx} & \sigma_{xy} & 0 \\ \sigma_{yx} & \sigma_{yy} & 0 \\ 0 & 0 & \sigma_{zz} \end{bmatrix},$$
$$\bar{\bar{\epsilon}} = \begin{bmatrix} \bar{\bar{\epsilon}}_s & 0 \\ 0 & \epsilon_{zz} \end{bmatrix} = \begin{bmatrix} \epsilon_{xx} & \epsilon_{xy} & 0 \\ \epsilon_{yx} & \epsilon_{yy} & 0 \\ 0 & 0 & \epsilon_{zz} \end{bmatrix} \quad (1)$$

where $\bar{\bar{\sigma}}_s$ and $\bar{\bar{\epsilon}}_s$ are 2×2 tensors. $\xi_{xx} = \xi'_{xx}\cos^2\alpha + \xi'_{yy}\sin^2\alpha$, $\xi_{xy} = \xi_{yx} = (\xi'_{yy} - \xi'_{xx})\sin\alpha\cos\alpha$, $\xi_{yy} = \xi'_{xx}\sin^2\alpha + \xi'_{yy}\cos^2\alpha$, and $\xi_{zz} = \xi'_{zz}$ with ξ be either ϵ or σ. We also assume an isotropic permeability of μ_o in all layers.

Decompose the $\bar{E}$ field, $\bar{H}$ field, and the curl operator into z component and s (x and y) components, substitute them into the Faraday's and the Ampere's laws, and look for a solution with the xy dependence of $\exp(i\bar{k}_s \cdot \bar{r}_s)$, we obtain the following state-variable equations [8]–[12]

$$\frac{dE_x}{dz} = \frac{k_x k_y}{\sigma_{zz} - i\omega\epsilon_{zz}} H_x + \left(i\omega\mu_o - \frac{k_x^2}{\sigma_{zz} - i\omega\epsilon_{zz}}\right) H_y$$
$$\frac{dE_y}{dz} = \left(-i\omega\mu_o + \frac{k_y^2}{\sigma_{zz} - i\omega\epsilon_{zz}}\right) H_x - \frac{k_x k_y}{\sigma_{zz} - i\omega\epsilon_{zz}} H_y$$
$$\frac{dH_x}{dz} = \left(\sigma_{yx} - i\omega\epsilon_{yx} - i\frac{k_x k_y}{\omega\mu_o}\right) E_x + \left(\sigma_{yy} - i\omega\epsilon_{yy} + i\frac{k_x^2}{\omega\mu_o}\right) E_y$$
$$\frac{dH_y}{dz} = \left(-\sigma_{xx} + i\omega\epsilon_{xx} - i\frac{k_y^2}{\omega\mu_o}\right) E_x + \left(-\sigma_{xy} + i\omega\epsilon_{xy} + i\frac{k_x k_y}{\omega\mu_o}\right) E_y. \quad (2)$$

The above equation can be solved numerically so that the tangential field components at different z's are related by a transition matrix as

$$\bar{V}(\bar{k}_s, z) = \bar{\bar{P}}(\bar{k}_s, z, 0) \cdot \bar{V}(\bar{k}_s, 0) \quad (3)$$

where

$$\bar{V}(\bar{k}_s, z) = [E_x(\bar{k}_s, z), E_y(\bar{k}_s, z), H_x(\bar{k}_s, z), H_y(\bar{k}_s, z)]^t \quad (4)$$

III. Microstrip Propagation Characteristics

For the microstrip line structure with laminated ground plane as shown in Fig. 1, the z-component of the fields in each region can be expressed as

$$E_{0z} = \int_{-\infty}^{\infty} dk_x e^{i\bar{k}_s \cdot \bar{r}_s} e_0(\bar{k}_s) e^{ik_{0z}z_0}$$
$$H_{0z} = \int_{-\infty}^{\infty} dk_x e^{i\bar{k}_s \cdot \bar{r}_s} h_0(\bar{k}_s) e^{ik_{0z}z_0}$$
$$E_{1z} = \int_{-\infty}^{\infty} dk_x e^{i\bar{k}_s \cdot \bar{r}_s} \times \left[e_1^U(\bar{k}_s) e^{ik_{1z}z_1} + e_1^D(\bar{k}_s) e^{-ik_{1z}z_1}\right]$$
$$H_{1z} = \int_{-\infty}^{\infty} dk_x e^{i\bar{k}_s \cdot \bar{r}_s} \times \left[h_1^U(\bar{k}_s) e^{ik_{1z}z_1} + h_1^D(\bar{k}_s) e^{-ik_{1z}z_1}\right]$$
$$E_{3z} = \int_{-\infty}^{\infty} dk_x e^{i\bar{k}_s \cdot \bar{r}_s} e_3(\bar{k}_s) e^{-ik_{3z}z_3}$$
$$H_{3z} = \int_{-\infty}^{\infty} dk_x e^{i\bar{k}_s \cdot \bar{r}_s} h_3(\bar{k}_s) e^{-ik_{3z}z_3} \quad (5)$$

where $\bar{k}_s = \hat{x}k_x + \hat{y}k_y$, $z_0 = z$, $z_1 = z+d$, and $z_3 = z+d+h$. Assume that the wave modes propagate in the y direction, then we have $k_y = \beta + i\alpha$ where β is the phase constant and α is the attenuation constant.

At $z = 0$, $\bar{E}_{0s} = \bar{E}_{1s}$ implies

$$\begin{bmatrix} \frac{k_{0z}}{k_s} e_0 \\ \frac{\omega\mu_o}{k_s} h_0 \end{bmatrix} = \begin{bmatrix} \frac{k_{1z}}{k_s}\cos(k_{1z}d)(e_1^U - e_1^D) + i\frac{k_{1z}}{k_s}\sin(k_{1z}d)(e_1^U + e_1^D) \\ \frac{\omega\mu_o}{k_s}\cos(k_{1z}d)(h_1^U + h_1^D) + i\frac{\omega\mu_o}{k_s}\sin(k_{1z}d)(h_1^U - h_1^D) \end{bmatrix}. \quad (6)$$

At $z = 0$, the discontinuities of magnetic fields account for the surface current as $\bar{J}_s(\bar{r}_s) = \hat{n} \times [\bar{H}_{0s}(z = 0+) - \bar{H}_{1s}(z = 0-)]$. Hence, we have (7), shown at the bottom of the page,

$$\bar{J}_s(\bar{r}_s) = \int_{-\infty}^{\infty} dk_x e^{i\bar{k}_s \cdot \bar{r}_s} \bar{\bar{F}}(\bar{k}_s) \cdot \begin{bmatrix} \frac{\omega\epsilon_0}{k_s} e_0 - \frac{\omega\epsilon_1}{k_s}\cos(k_{1z}d)(e_1^U + e_1^D) - i\frac{\omega\epsilon_1}{k_s}\sin(k_{1z}d)(e_1^U - e_1^D) \\ \frac{k_{0z}}{k_s} h_0 - \frac{k_{1z}}{k_s}\cos(k_{1z}d)(h_1^U - h_1^D) - i\frac{k_{1z}}{k_s}\sin(k_{1z}d)(h_1^U + h_1^D) \end{bmatrix} \quad (7)$$

where

$$\bar{\bar{F}}(\bar{k}_s) = \frac{1}{k_s}\begin{bmatrix} k_x & k_y \\ k_y & -k_x \end{bmatrix}. \tag{8}$$

The tangential field components at $z = z_N = -d$ and $z = z_0 = -d - h$ are related by the transition matrix as

$$\begin{aligned}
&\bar{\bar{F}}(\bar{k}_s)\cdot\begin{bmatrix} -\frac{k_{1z}}{k_s}(e_1^U - e_1^D) \\ -\frac{\omega\mu_o}{k_s}(h_1^U + h_1^D)\end{bmatrix} \\
&\quad = \bar{\bar{P}}_{11}\cdot\bar{\bar{F}}(\bar{k}_s)\cdot\begin{bmatrix} \frac{k_{3z}}{k_s}e_3(\bar{k}_s) \\ -\frac{\omega\mu_o}{k_s}h_3(\bar{k}_s)\end{bmatrix} \\
&\qquad + \bar{\bar{P}}_{12}\cdot\bar{\bar{F}}(\bar{k}_s)\cdot\begin{bmatrix} \frac{k_{3z}}{k_s}h_3(\bar{k}_s) \\ \frac{\omega\epsilon_3}{k_s}e_3(\bar{k}_s)\end{bmatrix} \\
&\bar{\bar{F}}(\bar{k}_s)\cdot\begin{bmatrix} -\frac{k_{1z}}{k_s}(h_1^U - h_1^D) \\ \frac{\omega\epsilon_1}{k_s}(e_1^U + e_1^D)\end{bmatrix} \\
&\quad = \bar{\bar{P}}_{21}\cdot\bar{\bar{F}}(\bar{k}_s)\cdot\begin{bmatrix} \frac{k_{3z}}{k_s}e_3(\bar{k}_s) \\ -\frac{\omega\mu_o}{k_s}h_3(\bar{k}_s)\end{bmatrix} \\
&\qquad + \bar{\bar{P}}_{22}\cdot\bar{\bar{F}}(\bar{k}_s)\cdot\begin{bmatrix} \frac{k_{3z}}{k_s}h_3(\bar{k}_s) \\ \frac{\omega\epsilon_3}{k_s}e_3(\bar{k}_s)\end{bmatrix}
\end{aligned} \tag{9}$$

where

$$\bar{\bar{P}}(\bar{k}_s, z_N, z_0) = \begin{bmatrix} \bar{\bar{P}}_{11}(\bar{k}_s, z_N, z_0) & \bar{\bar{P}}_{12}(\bar{k}_s, z_N, z_0) \\ \bar{\bar{P}}_{21}(\bar{k}_s, z_N, z_0) & \bar{\bar{P}}_{22}(\bar{k}_s, z_N, z_0)\end{bmatrix}. \tag{10}$$

Eliminating the unknowns e_0, h_0, e_1^U, e_1^D, h_1^U, h_1^D, e_3, and h_3 from (6), (7), and (9), the tangential electric field at $z = 0$ can be related to the patch surface current as

$$\bar{E}_{0s}(\bar{r}_s) = \int_{-\infty}^{\infty} dk_x e^{\imath\bar{k}_s\cdot\bar{r}_s}\bar{\bar{G}}(\bar{k}_s, z_0)\cdot\bar{J}_s(k_x). \tag{11}$$

Details of derivation can be found in Appendix A.
Next, impose the boundary condition that

$$\begin{aligned}
\bar{J}_s(\bar{r}_s) &= 0, \quad \text{outside of the strip} \\
\bar{E}_{0s}(\bar{r}_s) &= 0, \quad \text{on the strip surface.}
\end{aligned} \tag{12}$$

Equation (12) is the dual vector integral equation to be solved for the dispersion relation.

IV. Galerkin's Method

The surface current $\bar{J}_s(\bar{r}_s)$ can be expressed as $\bar{J}_s(x)e^{\imath k_y y}$. For a microstrip of width a, we choose a set of basis functions to represent $\bar{J}_s(x)$ as

$$\bar{J}_s(x) = \sum_{n=1}^{N} a_n\hat{x}f_{xn}(x) + \sum_{m=0}^{M} b_m\hat{y}f_{ym}(x) \tag{13}$$

where

$$\begin{aligned}
f_{xn}(x) &= \begin{cases}\sin[\frac{n\pi}{a}(x + a/2)], & |x| \le a/2 \\ 0, & \text{elsewhere}\end{cases} \\
f_{ym}(x) &= \begin{cases}\frac{\cos[\frac{m\pi}{a}(x+a/2)]}{\sqrt{(a/2)^2 - x^2}}, & |x| \le a/2 \\ 0, & \text{elsewhere.}\end{cases}
\end{aligned} \tag{14}$$

Taking the Fourier transform of (13), and substituting into (12), we have

$$\begin{aligned}
&\int_{-\infty}^{\infty} dk_x e^{\imath\bar{k}_s\cdot\bar{r}_s}\bar{\bar{G}}(\bar{k}_s, z_0 = 0) \\
&\quad\cdot\left[\sum_{n=1}^{N} a_n\hat{x}f_{xn}(k_x) + \sum_{m=0}^{M} b_m\hat{y}f_{ym}(k_x)\right] = 0.
\end{aligned} \tag{15}$$

Next, we choose another set of weighting functions

$$\begin{aligned}
g_{xk}(x) &= \begin{cases}\sin[\frac{k\pi}{a}(x + a/2)], & |x| \le a/2 \\ 0, & \text{elsewhere}\end{cases} \\
g_{yl}(x) &= \begin{cases}\cos[\frac{l\pi}{a}(x + a/2)], & |x| \le a/2 \\ 0, & \text{elsewhere.}\end{cases}
\end{aligned} \tag{16}$$

Taking the inner product of $\hat{x}g_{xk}(x)e^{-\imath k_y y}$ $(1 \le k \le N)$ and $\hat{y}g_{yl}(x)e^{-\imath k_y y}$ $(0 \le l \le M)$ with (15), we have

$$\begin{aligned}
&\sum_{n=1}^{N} a_n\int_{-\infty}^{\infty} dk_x g_{xk}(-k_x)\hat{x}\cdot\bar{\bar{G}}(\bar{k}_s, z_0 = 0)\cdot xf_{xn}(k_x) \\
&\quad + \sum_{m=0}^{M} b_m\int_{-\infty}^{\infty} dk_x g_{xk}(-k_x)\hat{x}\cdot\bar{\bar{G}}(\bar{k}_s, z_0 = 0)\cdot\hat{y}f_{ym}(k_x) \\
&\quad = 0, \qquad 1 \le k \le N \\
&\sum_{n=1}^{N} a_n\int_{-\infty}^{\infty} dk_x g_{yl}(-k_x)\hat{y}\cdot\bar{\bar{G}}(\bar{k}_s, z_0 = 0)\cdot\hat{x}f_{xn}(k_x) \\
&\quad + \sum_{m=0}^{M} b_m\int_{-\infty}^{\infty} dk_x g_{yl}(-k_x)\hat{y}\cdot\bar{\bar{G}}(\bar{k}_s, z_0 = 0)\cdot\hat{y}f_{ym}(k_x) \\
&\quad = 0, \qquad 0 \le l \le M.
\end{aligned} \tag{17}$$

Equation (17) constitutes a determinantal equation to be solved for k_y at a given frequency ω.

V. Coupling Through Ground Plane

Consider a symmetrical structure as shown in Fig. 2 in which both the even and the odd modes exist. For the even mode, the longitudinal current J_y on both strips are in phase, hence $\bar{H}_s$ vanishes in the midplane. We may solve an equivalent problem with a perfect magnetic conductor at the midplane. Likewise, we may solve an equivalent problem with a perfect electric conductor at the midplane for the odd mode. The difference of k_y between the even and the odd modes indicates the coupling effect through the laminated ground plane.

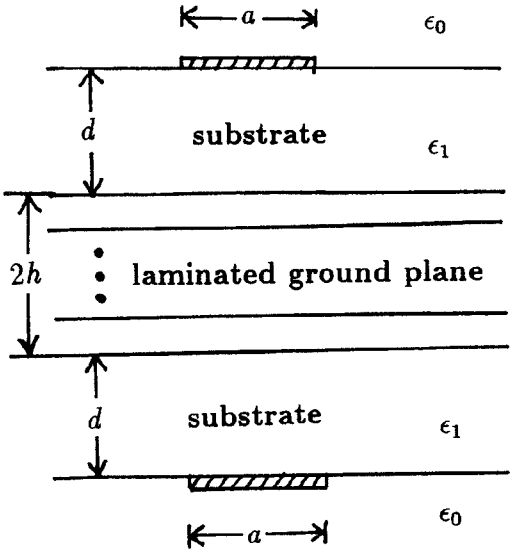

(a)

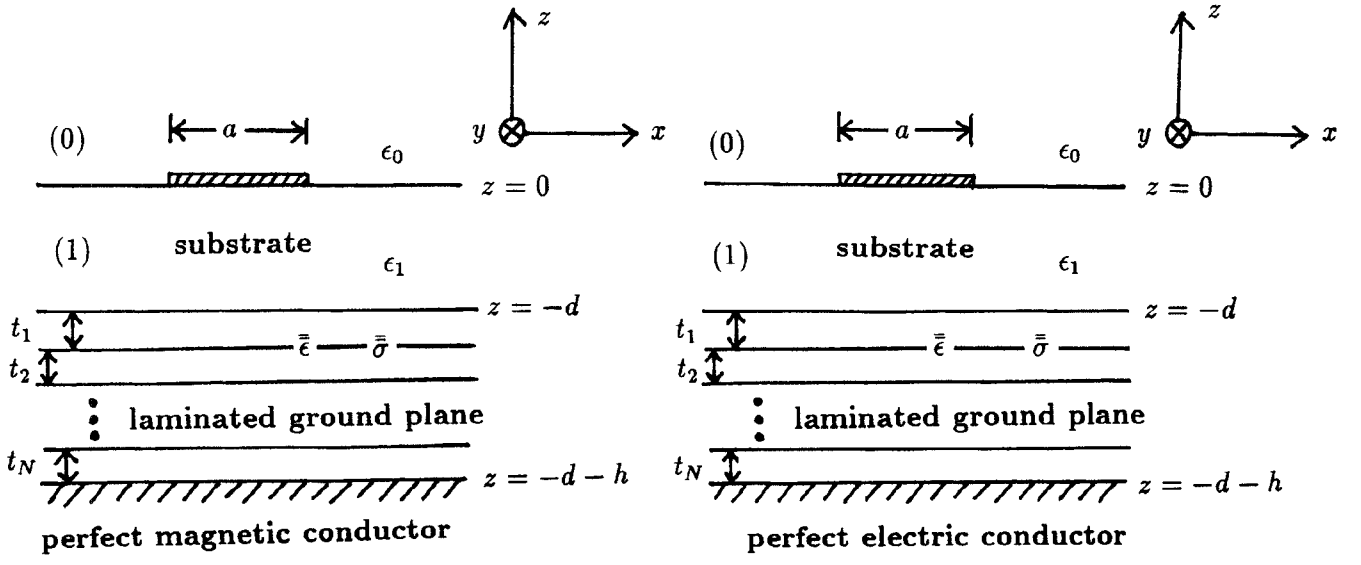

(b) (c)

Fig. 2. (a) Two symmetrical microstrip lines coupling through a laminated ground plane. (b) Equivalent problem for the even mode. (c) Equivalent problem for the odd mode.

The definitions of matrices in this section can be found in Appendix B. Following the same procedures as in Section III for the even mode

$$\begin{bmatrix} e_1^U - e_1^D \\ h_1^U + h_1^D \end{bmatrix} = \bar{\bar{R}}^{(e)} \cdot \begin{bmatrix} e_x \\ e_y \end{bmatrix}, \quad \begin{bmatrix} h_1^U - h_1^D \\ e_1^U + e_1^D \end{bmatrix} = \bar{\bar{S}}^{(e)} \cdot \begin{bmatrix} e_x \\ e_y \end{bmatrix} \tag{18}$$

where $[e_x, e_y]^t$ is the Fourier transform of $\bar{E}_s$ at the midplane. For the odd mode

$$\begin{bmatrix} e_1^U - e_1^D \\ h_1^U + h_1^D \end{bmatrix} = \bar{\bar{R}}^{(o)} \cdot \begin{bmatrix} h_x \\ h_y \end{bmatrix}, \quad \begin{bmatrix} h_1^U - h_1^D \\ e_1^U + e_1^D \end{bmatrix} = \bar{\bar{S}}^{(o)} \cdot \begin{bmatrix} h_x \\ h_y \end{bmatrix} \tag{19}$$

where $[h_x, h_y]^t$ is the Fourier transform of $\bar{H}_s$ at the midplane. Imposing the boundary condition that $\bar{E}_s$ is continuous at $z = 0$

$$\begin{bmatrix} e_0 \\ h_0 \end{bmatrix} = \bar{\bar{T}}^{(\alpha)} \cdot \begin{bmatrix} c_x \\ c_y \end{bmatrix} \tag{20}$$

where $c = e$ when $\alpha = e$, and $c = h$ when $\alpha = o$.

The surface current at $z = 0$ accounts for the discontinuity of $\bar{H}_s$, and can be expressed as

$$\bar{J}_s(\bar{r}_s) = \int_{-\infty}^{\infty} dk_x e^{i\bar{k}_s \cdot \bar{r}_s} \bar{\bar{F}}(\bar{k}_s) \cdot \bar{\bar{X}}^{(\alpha)} \cdot \begin{bmatrix} c_x \\ c_y \end{bmatrix}. \tag{21}$$

Similarly, $\bar{E}_{0s}$ can be expressed as

$$\bar{E}_{0s}(\bar{r}_s) = \int_{-\infty}^{\infty} dk_x e^{i\bar{k}_s \cdot \bar{r}_s} \bar{\bar{G}}^{(\alpha)}(\bar{k}_s, z_0) \cdot \bar{J}_s(k_x). \tag{22}$$

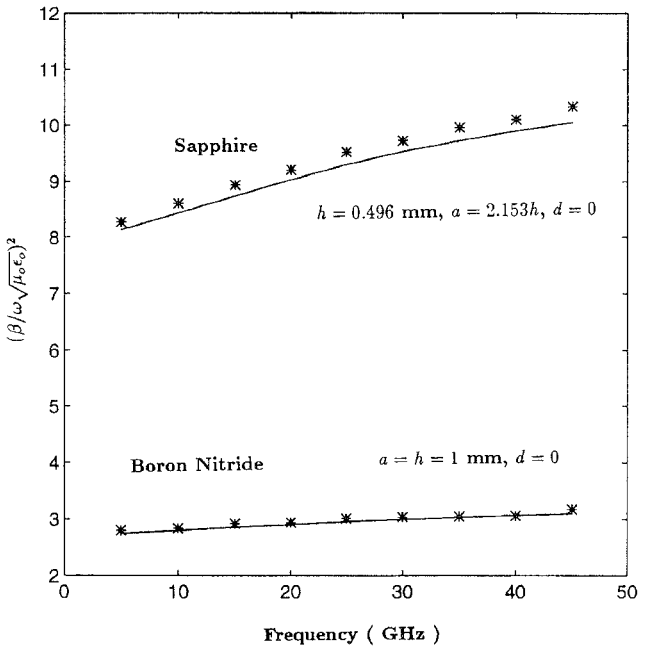

Fig. 3. Frequency dependence of effective dielectric constant for a single microstrip line on sapphire or boron nitride (—this method, ** data from [7]). For sapphire, $\epsilon'_{xx} = \epsilon'_{yy} = 9.4\epsilon_o$. $\epsilon'_{zz} = 11\ 6\epsilon_o$. For boron nitride, $\epsilon'_{xx} = \epsilon'_{yy} = 5\ 12\epsilon_o$, $\epsilon'_{zz} = 3.4\epsilon_o$.

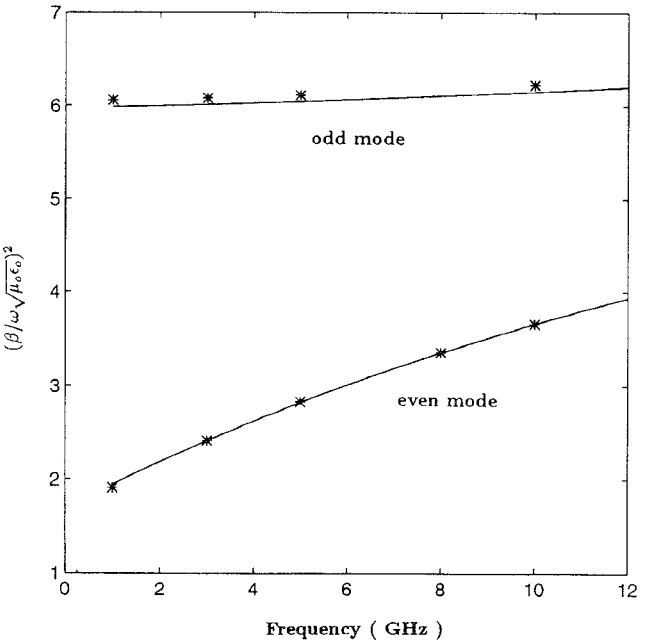

Fig. 4. Effective dielectric constant of two symmetrical microstrip lines coupling through a substrate of thickness $2h = 1\ 28$ mm, $a = 0.1$ mm, $d = 0$. $\epsilon'_{xx} = \epsilon'_{yy} = \epsilon'_{zz} = 9\ 9\epsilon_o$(—this method, ** data from [15])

Finally, impose the boundary condition as in (12) and use the Galerkin's procedure to solve for the dispersion relation for the even and the odd modes.

VI. Results and Discussions

We first verify our method by comparing effective dielectric constants with literatures. To model the configuration in [7], replace region (3) by a perfect electric conductor, and reduce the thickness of region (1) to zero. The computed effective dielectric constant of a single microstrip line is close to the data in [7].

In Fig. 4, we compare the effective dielectric constants of two symmetrical microstrip lines with the data in [15]. The thickness of region (1) is reduced to zero. Our results match reasonably well with reference data.

Floquet modes approach is used in [4], where the fiber spacing considered is around 0.1 to 0.5 wavelengths in the resin matrix. The accuracy of permittivity and conductivity tensor approximation in [5] render more accurate results when the fiber spacing is smaller in terms of wavelength in the resin matrix. If we estimate that fiber spacing be at most five thousandths of a wavelength in the resin for the permittivity and conductivity tensors to be a fair approximation, then the highest frequency our approach can be applied to G/E composite is around 8 GHz if the fiber spacing is around 100 μm.

We then analyze the propagation properties of a microstrip line. In Figs. 5 and 6, we show the phase and attenuation constants of a microstrip line with laminated ground plane and with a 1 μm-thick solid copper ground plane. The phase constant with laminated ground plane increases as frequency decreases, which implies a slower propagation speed. The attenuation constant in both cases increases as the frequency decreases. The microstrip line with laminated ground plane has a higher attenuation constant than the other line. We also study the effect of substrate dielectric constant ϵ_1, and observe that substrate having higher dielectric constant gives higher attenuation rate.

Next, we study the coupling between two symmetrical microstrip lines on opposite sides of a laminated ground plane. The phase constants of the even and the odd modes differ slightly. However, as shown in Fig. 7, the attenuation rate of the even mode is higher than that of the odd mode especially in the low frequency range.

In Figs. 8 and 9, we show the effect of substrate dielectric constant on the propagation properties. The phase constant of the even mode increases as frequency is decreased from 500 MHz. The even mode has a higher attenuation constant than the odd mode, and the attenuation constant of both modes increases as the substrate dielectric constant increases.

Finally, we study the effect of lamina conductivity on the propagation properties. Assume that in each lamina, the conductivity perpendicular to the wire/fiber orientation is 50 $\mho$/m, and the conductivity along the wire/fiber is varied from $10^4\mho$/m to $2 \times 10^7\mho$/m. We observe that the phase constants of both modes are insensitive to the conductivity variation. The attenuation constant of the even mode decreases monotonically with conductivity, while the odd mode attenuation constant reaches a maximum around $10^6\mho$/m. The attenuation constant increases with the substrate dielectric constant. Similar results are observed if we increase the number of laminae instead of increasing the lamina conductivity.

In numerical computation, attention should be paid when: 1) there are too many composite layers; 2) lamina(e) is too

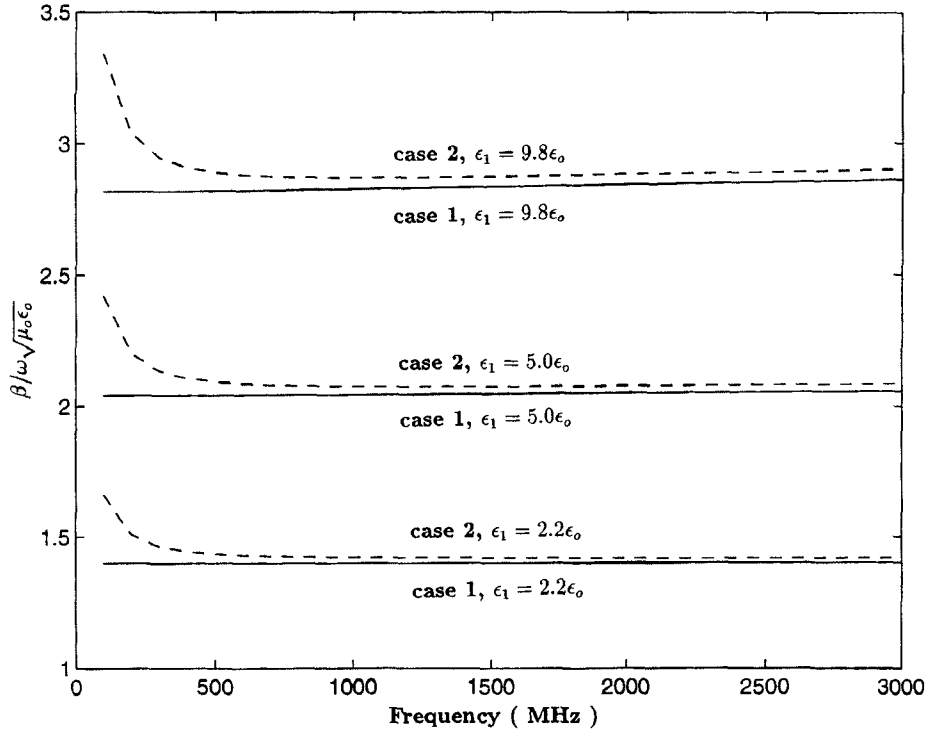

Fig. 5. Phase constant of a microstrip line, $a = 5$ mm, $d = 1$ mm, $\epsilon_0 = \epsilon_3 = \epsilon_o$, case 1 (one lamina of solid copper ground plane): $t_1 = 1$ μm, $\epsilon'_{xx} = \epsilon'_{yy} = \epsilon'_{zz} = \epsilon_o$, $\sigma'_{xx} = \sigma'_{yy} = \sigma'_{zz} = 5.8 \times 10^7$ Ʊ/m; case 2 (two laminae of composites): $t_1 = t_2 = 25.4$ μm, $\alpha_1 = 0°$, $\alpha_2 = 90°$, $\epsilon'_{yx} = \epsilon'_{yy} = \epsilon'_{zz} = \epsilon_o$, $\sigma'_{yx} = 4 \times 10^4$ Ʊ/m, $\sigma'_{yy} = \sigma'_{zz} = 50$ Ʊ/m.

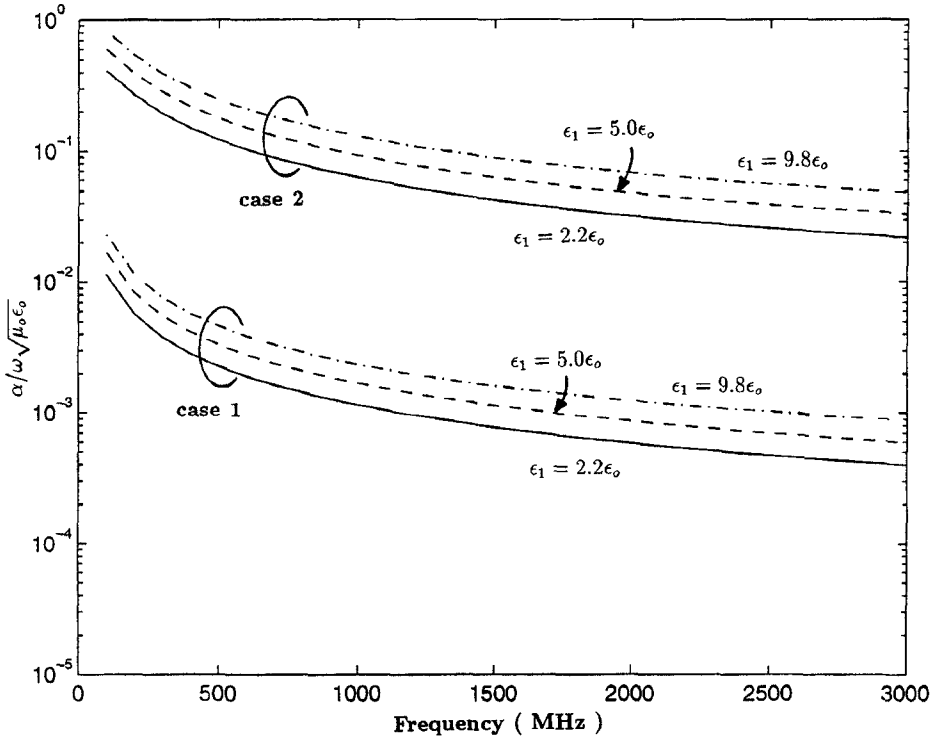

Fig. 6. Attenuation constant of a microstrip line with solid copper or laminated ground plane, the parameters are the same as in Fig. 5.

thick; or 3) laminate conductivity is too high. We may define a skin depth $\delta_m = \sqrt{2/\omega\mu_o\sigma_m}$ to estimate field penetration into laminated media, where σ_m is the maximum of σ'_{xx}, σ'_{yy}, and σ'_{zz}. We observe that when the total laminate thickness is larger than $10\delta_m$, some irregular variations may appear, indicating that numerial accuracy is deteriorated by truncation

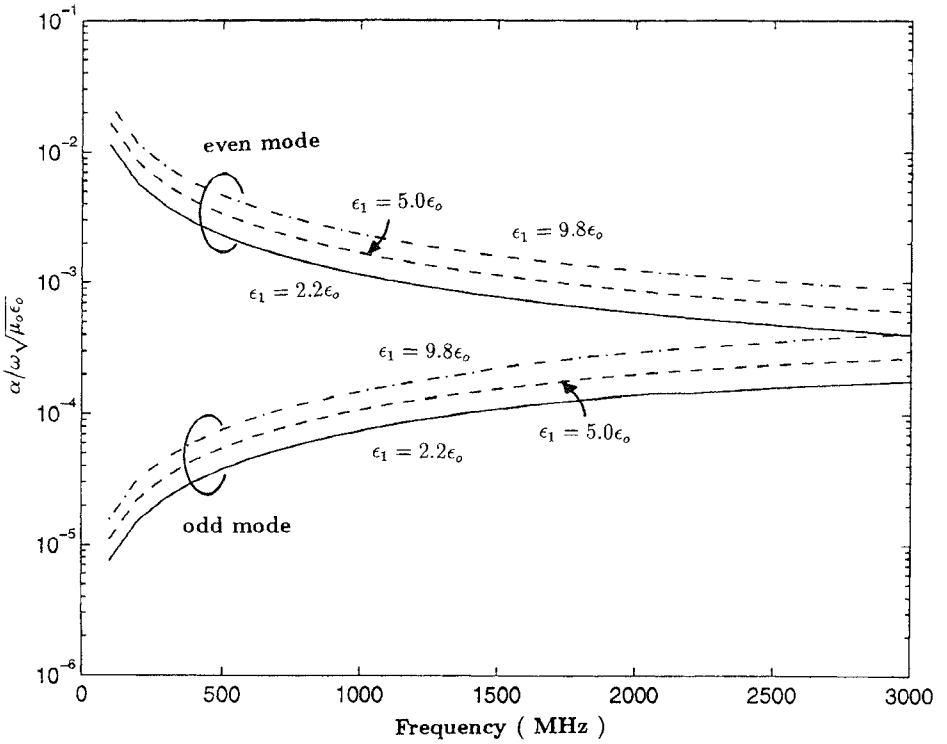

Fig 7 Attenuation constant of two symmetrical microstrip lines coupling through one lamina of solid copper ground plane, $a = 5$ mm, $d = 1$ mm, $\epsilon_0 = \epsilon_3 = \epsilon_o$, $t_1 = 1$ μm, $\epsilon'_{xx} = \epsilon'_{yy} = \epsilon'_{zz} = \epsilon_o$, $\sigma'_{xx} = \sigma'_{yy} = \sigma'_{zz} = 5.8 \times 10^7$ U/m.

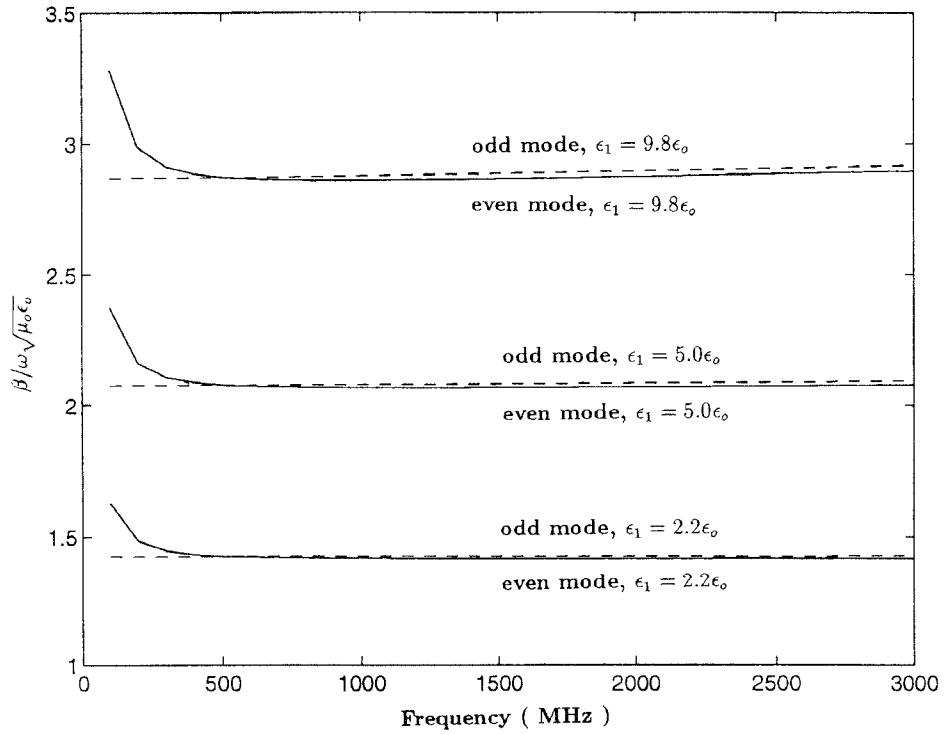

Fig. 8. Phase constant of two symmetrical microstrip lines coupling through four-lamina ground plane, $a = 5$ mm, $d = 1$ mm, $\epsilon_0 = \epsilon_3 = \epsilon_o$, $t_1 = t_2 = t_3 = t_4 = 12.7$ μm, $\alpha_1 = 0°$, $\alpha_2 = 45°$, $\alpha_3 = 90°$, $\alpha_4 = 135°$, $\epsilon'_{xx} = \epsilon'_{yy} = \epsilon'_{zz} = \epsilon_o$, $\sigma'_{xx} = 4 \times 10^4$ U/m, $\sigma'_{yy} = \sigma'_{zz} = 50$ U/m.

errors. It is related to the fact that when the laminated media is too thick in terms of skin depth δ_m, coupling between the fields on planes $z = -d$ and $z = -d - h$ becomes too weak. The laminate thickness associated with the results presented in this paper is thinner than $10\delta_m$ at the highest frequency considered.

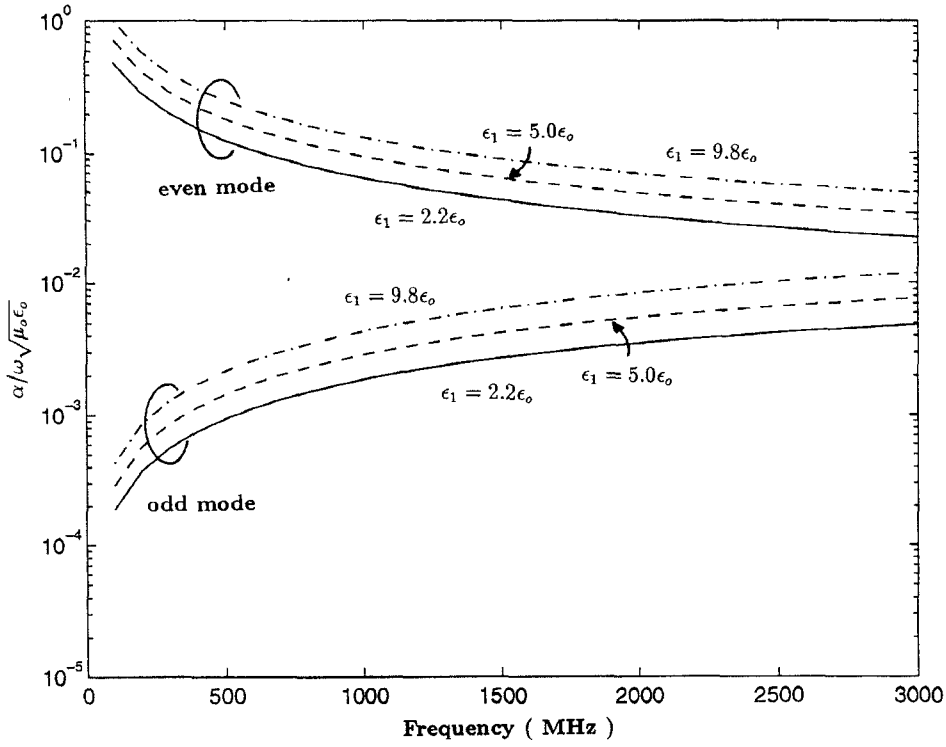

Fig. 9. Attenuation constant of two symmetrical microstrip lines coupling through four-lamina ground plane, the parameters are the same as in Fig. 8.

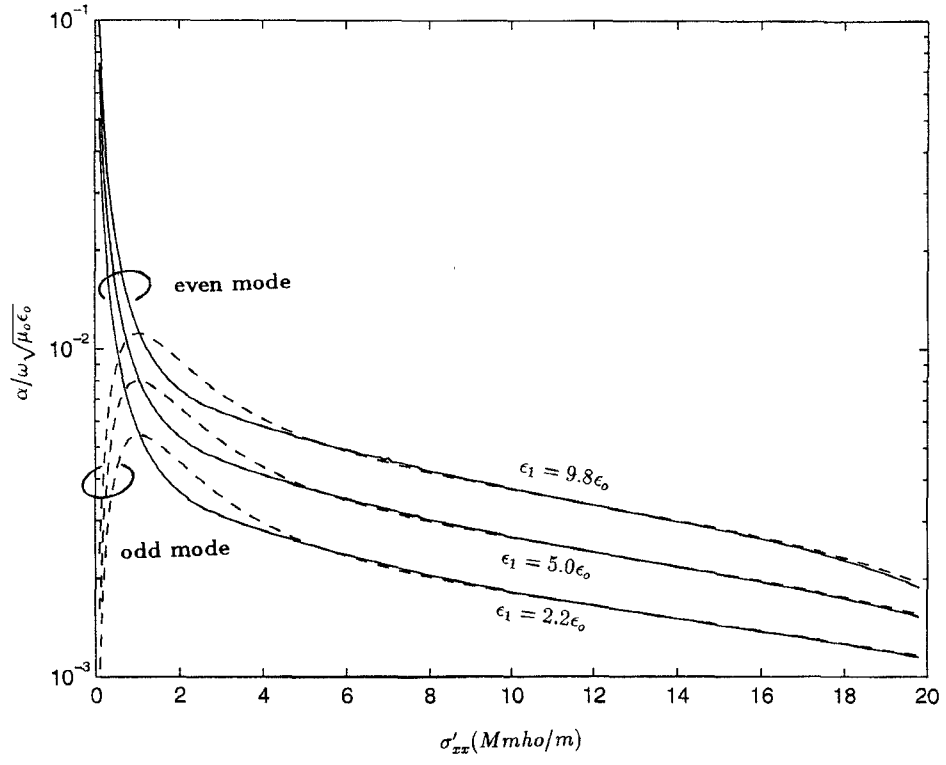

Fig. 10. Attenuation constant of two symmetrical microstrip lines coupling through two-lamina ground plane, $f = 500$ MHz, $a = 5$ mm, $d = 1$ mm, $\epsilon_0 = \epsilon_3 = \epsilon_o$, $t_1 = t_2 = 25.4$ μm, $\alpha_1 = 0°$, $\alpha_2 = 90°$, $\epsilon'_{xx} = \epsilon'_{yy} = \epsilon'_{zz} = \epsilon_o$, $\sigma'_{yy} = \sigma'_{zz} = 50\mho$/m.

VII. Conclusion

We use a transition matrix to incorporate the effect of laminated ground plane into our integral equation formulation. Galerkin's method is applied to solve for the dispersion relation of microstrip lines. The coupling effect is analyzed by comparing the even and the odd modes of two symmetrical microstrip lines on opposite sides of the laminated ground

plane. The phase constant is less sensitive to the ground plane except in the low frequency range. The attenuation constant has a wider range of variation as the lamina conductivity and the frequency are changed. The results are useful in designing circuit board and in studying signal transmission in lamina environment.

APPENDIX A

In this Appendix, we present the details of deriving the relation between the tangential electric field at $z = 0$ and the patch surface current. Multiplying (9) by $\bar{\bar{F}}(\bar{k}_s)$ and defining $\bar{\bar{Q}}_{ij} = \bar{\bar{F}}(\bar{k}_s) \cdot \bar{\bar{P}}_{ij} \cdot \bar{\bar{F}}(\bar{k}_s)$ with $1 \le i, j \le 2$, we have

$$\begin{aligned}
&\begin{bmatrix} -\frac{k_{1z}}{k_s}(e_1^U - e_1^D) \\ -\frac{\omega\mu_o}{k_s}(h_1^U + h_1^D) \end{bmatrix} \\
&\quad = \bar{\bar{Q}}_{11} \cdot \begin{bmatrix} \frac{k_{3z}}{k_s} e_3(\bar{k}_s) \\ -\frac{\omega\mu_o}{k_s} h_3(\bar{k}_s) \end{bmatrix} + \bar{\bar{Q}}_{12} \cdot \begin{bmatrix} \frac{k_{3z}}{k_s} h_3(\bar{k}_s) \\ \frac{\omega\epsilon_3}{k_s} e_3(\bar{k}_s) \end{bmatrix} \\
&\begin{bmatrix} -\frac{k_{1z}}{k_s}(h_1^U - h_1^D) \\ \frac{\omega\epsilon_1}{k_s}(e_1^U + e_1^D) \end{bmatrix} \\
&\quad = \bar{\bar{Q}}_{21} \cdot \begin{bmatrix} \frac{k_{3z}}{k_s} e_3(\bar{k}_s) \\ -\frac{\omega\mu_o}{k_s} h_3(\bar{k}_s) \end{bmatrix} + \bar{\bar{Q}}_{22} \cdot \begin{bmatrix} \frac{k_{3z}}{k_s} h_3(\bar{k}_s) \\ \frac{\omega\epsilon_3}{k_s} e_3(\bar{k}_s) \end{bmatrix}.
\end{aligned} \tag{23}$$

Solve (23) to have

$$\begin{bmatrix} e_1^U - e_1^D \\ h_1^U + h_1^D \end{bmatrix} = \bar{\bar{R}} \cdot \begin{bmatrix} e_3 \\ h_3 \end{bmatrix}, \quad \begin{bmatrix} h_1^U - h_1^D \\ e_1^U + e_1^D \end{bmatrix} = \bar{\bar{S}} \cdot \begin{bmatrix} e_3 \\ h_3 \end{bmatrix}. \tag{24}$$

Substituting (24) into (6), we obtain

$$\begin{bmatrix} e_0 \\ h_0 \end{bmatrix} = \bar{\bar{T}} \cdot \begin{bmatrix} e_3 \\ h_3 \end{bmatrix}. \tag{25}$$

Next, substitute (24) and (25) into (7) to have

$$\begin{aligned}
\bar{J}_s(\bar{r}_s) &= \int_{-\infty}^{\infty} dk_x e^{i\bar{k}_s \cdot \bar{r}_s} \bar{J}_s(k_x) \\
&= \int_{-\infty}^{\infty} dk_x e^{i\bar{k}_s \cdot \bar{r}_s} \bar{\bar{F}}(\bar{k}_s) \cdot \bar{\bar{X}} \cdot \begin{bmatrix} e_3 \\ h_3 \end{bmatrix}
\end{aligned} \tag{26}$$

where it becomes as (27), shown at the bottom of the page. From (25) and (26), $\bar{E}_{0s}$ can be expressed as

$$\begin{aligned}
\bar{E}_{0s}(\bar{r}_s) &= \int_{-\infty}^{\infty} dk_x e^{i\bar{k}_s \cdot \bar{r}_s} e^{ik_{0z}z_0} \bar{\bar{F}}(\bar{k}_s) \cdot \begin{bmatrix} -\frac{k_{0z}}{k_s} & 0 \\ 0 & -\frac{\omega\mu_o}{k_s} \end{bmatrix} \\
&\quad \cdot \bar{\bar{T}} \cdot \bar{\bar{X}}^{-1} \cdot \bar{\bar{F}}(\bar{k}_s) \cdot \bar{J}_s(k_x) \\
&= \int_{-\infty}^{\infty} dk_x e^{i\bar{k}_s \cdot \bar{r}_s} \bar{\bar{G}}(\bar{k}_s, z_0) \cdot \bar{J}_s(k_x).
\end{aligned} \tag{28}$$

APPENDIX B

In this Appendix, we list the matrices used in deriving the integral equation in Section V.

$$\bar{\bar{R}}^{(e)} = -\begin{bmatrix} \frac{k_s}{k_{1z}} & 0 \\ 0 & \frac{k_s}{\omega\mu_o} \end{bmatrix} \cdot \bar{\bar{F}}(\bar{k}_s) \cdot \bar{\bar{P}}_{11},$$

$$\bar{\bar{S}}^{(e)} = \begin{bmatrix} -\frac{k_s}{k_{1z}} & 0 \\ 0 & \frac{k_s}{\omega\epsilon_1} \end{bmatrix} \cdot \bar{\bar{F}}(\bar{k}_s) \cdot \bar{\bar{P}}_{21} \tag{29}$$

$$\bar{\bar{R}}^{(o)} = -\begin{bmatrix} \frac{k_s}{k_{1z}} & 0 \\ 0 & \frac{k_s}{\omega\mu_o} \end{bmatrix} \cdot \bar{\bar{F}}(\bar{k}_s) \cdot \bar{\bar{P}}_{12},$$

$$\bar{\bar{S}}^{(o)} = \begin{bmatrix} -\frac{k_s}{k_{1z}} & 0 \\ 0 & \frac{k_s}{\omega\epsilon_1} \end{bmatrix} \cdot \bar{\bar{F}}(\bar{k}_s) \cdot \bar{\bar{P}}_{22} \tag{30}$$

$$\begin{aligned}
\bar{\bar{T}}^{(\alpha)} &= \cos(k_{1z}d) \begin{bmatrix} \frac{k_{1z}}{k_{0z}} & 0 \\ 0 & 1 \end{bmatrix} \cdot \bar{\bar{R}}^{(\alpha)} \\
&\quad + i\sin(k_{1z}d) \begin{bmatrix} 0 & \frac{k_{1z}}{k_{0z}} \\ 1 & 0 \end{bmatrix} \cdot \bar{\bar{S}}^{(\alpha)}
\end{aligned} \tag{31}$$

and as in (32), shown at the bottom of the page

$$\begin{aligned}
\bar{\bar{G}}^{(\alpha)}(\bar{k}_s, z_0) &= e^{ik_{0z}z_0} \bar{\bar{F}}(\bar{k}_s) \cdot \begin{bmatrix} -\frac{k_{0z}}{k_s} & 0 \\ 0 & -\frac{\omega\mu_o}{k_s} \end{bmatrix} \\
&\quad \cdot \bar{\bar{T}}^{(\alpha)} \cdot \left[\bar{\bar{X}}^{(\alpha)}\right]^{-1} \cdot \bar{\bar{F}}(\bar{k}_s).
\end{aligned} \tag{33}$$

ACKNOWLEDGMENT

The author would like to thank the reviewers for their precious comments.

$$\begin{aligned}
\bar{\bar{X}} = &\begin{bmatrix} \frac{\omega\epsilon_0}{k_s}\frac{k_{1z}}{k_{0z}}\cos(k_{1z}d) - i\frac{\omega\epsilon_1}{k_s}\sin(k_{1z}d) & 0 \\ 0 & \frac{k_{0z}}{k_s}\cos(k_{1z}d) - i\frac{k_{1z}}{k_s}\sin(k_{1z}d) \end{bmatrix} \cdot \bar{\bar{R}} \\
&+ \begin{bmatrix} 0 & i\frac{\omega\epsilon_0}{k_s}\frac{k_{1z}}{k_{0z}}\sin(k_{1z}d) - \frac{\omega\epsilon_1}{k_s}\cos(k_{1z}d) \\ i\frac{k_{0z}}{k_s}\sin(k_{1z}d) - \frac{k_{1z}}{k_s}\cos(k_{1z}d) & 0 \end{bmatrix} \cdot \bar{\bar{S}}.
\end{aligned} \tag{27}$$

$$\begin{aligned}
\bar{\bar{X}}^{(\alpha)} = &\begin{bmatrix} \frac{\omega\epsilon_0}{k_s}\frac{k_{1z}}{k_{0z}}\cos(k_{1z}d) - i\frac{\omega\epsilon_1}{k_s}\sin(k_{1z}d) & 0 \\ 0 & \frac{k_{0z}}{k_s}\cos(k_{1z}d) - i\frac{k_{1z}}{k_s}\sin(k_{1z}d) \end{bmatrix} \cdot \bar{\bar{R}}^{(\alpha)} \\
&+ \begin{bmatrix} 0 & i\frac{\omega\epsilon_0}{k_s}\frac{k_{1z}}{k_{0z}}\sin(k_{1z}d) - \frac{\omega\epsilon_1}{k_s}\cos(k_{1z}d) \\ i\frac{k_{0z}}{k_s}\sin(k_{1z}d) - \frac{k_{1z}}{k_s}\cos(k_{1z}d) & 0 \end{bmatrix} \cdot \bar{\bar{S}}^{(\alpha)}
\end{aligned} \tag{32}$$

REFERENCES

[1] B. J. Rubin and H. L. Bertoni, "Waves guided by conductive strips above a periodically perforated ground plane," *IEEE Trans. Microwave Theory Tech.*, vol. MTT-31, pp. 541–549, July 1983.

[2] C. H. Chan and R. Mittra, "The propagation characteristics of signal lines embedded in a multilayered structure in the presence of a periodically perforated ground plane," *IEEE Trans. Microwave Theory Tech.*, vol. MTT-36, pp. 968–975, June 1988.

[3] M. Kahrizi, T. K. Sarkar and Z. A. Maricevic, "Dynamic analysis of a microstrip line over a perforated ground plane," *IEEE Trans. Microwave Theory Tech.*, vol. 42, pp. 820–825, May 1994.

[4] L. N. Medgyesi-Mitschang and J. M. Putnam, "Scattering from composite laminate strips," *IEEE Trans. Antennas Propagat.*, vol. 37, pp. 1427–1436, Nov. 1989.

[5] M.-S. Lin and C. H. Chen, "Plane-wave shielding characteristics of anisotropic laminated composites," *IEEE Trans. Electromagn. Compat.*, vol. 35, pp. 21–27, Feb. 1993.

[6] E. Pillai and W. Wiesbeck, "Derivation of equivalent circuits for multilayer printed circuit board discontinuities using full wave models," *IEEE Trans. Microwave Theory Tech.*, vol. 42, pp. 1774–1783, Sept. 1994.

[7] Y. Chen and B. Beker, "Analysis of single and coupled microstrip lines on anisotropic substrates using differential matrix operators and the spectral-domain method," *IEEE Trans. Microwave Theory Tech.*, vol. 41, pp. 123–128, Jan. 1993.

[8] D. W. Berreman, "Optics in stratified and anisotropic media: 4×4-matrix formulation," *J. Opt. Soc. Am.*, vol. 62, pp. 502–510, Apr. 1972.

[9] O. Schwelb, "Stratified lossy anisotropic media: Genearal characteristics," *J. Opt. Soc. Am. A*, vol. 3, pp. 188–193, Feb. 1986.

[10] M. A. Morgan, D. L. Fisher and E. A. Milne, "Electromagnetic scattering by stratified inhomogeneous anisotropic media," *IEEE Trans. Antennas Propagat.*, vol. 35, pp. 191–197, Feb. 1987.

[11] C. M. Krowne, "Fourier transformed matrix method of finding propagation characteristics of complex anisotropic layered media," *IEEE Trans. Microwave Theory Tech.*, vol. MTT-32, pp. 1617–1625, Dec. 1984.

[12] J. L. Tsalamengas, "Interaction of electromagnetic waves with general bianisotropic slabs," *IEEE Trans. Microwave Theory Tech.*, vol. 40, pp. 1870–1878, Oct. 1992.

[13] G. G. Sanford, "Conformal microstrip phased array for aircraft tests with ATS-6," *IEEE Trans. Antennas Propagat.*, vol. AP-26, pp. 642–646, Sept. 1978.

[14] J. A. Kong, *Electromagnetic Wave Theory*, 2nd Ed. New York: Wiley, 1990.

[15] L. Gurel and W. C. Chew, "Guidance or resonance conditions for strips or disks embedded in homogeneous and layered media," *IEEE Trans. Microwave Theory Tech.*, vol. 36, pp. 1498–1506, Nov. 1988.

Jean-Fu Kiang (M'89) was born in Taipei, Taiwan, Republic of China, on February 2, 1957. He received the B.S.E.E and M.S.E.E degrees from National Taiwan University, and the Ph.D. degree from MIT in 1979, 1981, and 1989, respectively.

He was with IBM Watson Research Center, Bellcore, and Siemens. He is now with the Department of Electrical Engineering, National Chung-Hsing University, Taichung, Taiwan.